The Boreal Summer Intraseasonal Oscillation: Relationship between Northward and Eastward Movement of Convection

David M. Lawrence and Peter J. Webster

Program in Atmospheric and Oceanic Sciences, University of Colorado, Boulder, Colorado

(Manuscript received 20 February 2001, in final form 13 August 2001)

ABSTRACT

The summertime intraseasonal oscillation (ISO) is an important component of the south Asian monsoon. Lagged regressions of intraseasonally filtered (25–80 days) outgoing longwave radiation (OLR) reveal that centers of convection move both northward and eastward from the central equatorial Indian Ocean subsequent to the initiation of an ISO. Eastward movement of convection is also seen at Indian subcontinent latitudes (10°–20°N). Based on the regression results, the summertime ISO convection signal appears as a band tilting northwestward with latitude and stretching from the equator to about 20°N. Viewed along any meridian, convection appears to propagate northward while equatorial convection propagates to the east. To examine the robustness of the connection between eastward and northward movement, individual ISOs are categorized and composited relative to the strength of the large-scale eastward component of convection in the central equatorial Indian Ocean. It is found that the majority of ISOs that exhibit northward movement onto the Indian subcontinent (42 out of 54 ISOs, or 78%) also exhibit eastward movement into the western Pacific Ocean. It is also found that when convection in the central Indian Ocean is not followed within 10–20 days by convection in the western Pacific Ocean (12 out of 54 ISOs, or 22%), the independent northward movement of convection in the Indian Ocean region is somewhat stunted.

The link between the eastward and northward movement of convection is consistent with an interpretation of the summertime ISO in terms of propagating equatorial modes. The northward moving portion of convection is forced by surface frictional convergence into the low pressure center of the Rossby cell that is excited by equatorial ISO convection. A similar convergence pattern is seen for the northern winter ISO, but it does not generate poleward movement due to relatively cool SSTs underlying the surface convergence.

1. Introduction

The southwest or south Asian summer monsoon is marked by episodes of abundant precipitation (active periods) separated by periods of reduced rainfall (break periods). The transitions from active to break periods and vice versa evolve slowly such that there are typically three to four active periods over the course of a single monsoon season, May to September (Webster et al. 1998). Prolonged dry spells, if they occur during critical growth periods, may adversely affect crop development and growth, and hence yields (see e.g., Lal et al. 1999). Consequently, understanding the transitions, as well as the timing of rainy and dry spells, has sociological importance and is particularly relevant for farmers and water managers in south Asia since advance information of forthcoming active and break spells could theoretically be used to implement mitigating agricultural and water management strategies.

The low-frequency active/break cycles occur on timescales of about 30–40 days (Raghavan et al. 1975; Yasunari 1979, 1980, 1981; Krishnamurti and Subrahmanyam 1982; Lau and Chan 1986). Spectral peaks in monsoonal parameters have been found in the 30–40-day period band in a number of studies (e.g., Yasunari 1979, cloudiness; Cadet 1986, precipitable water; Knutson et al. 1986, outgoing longwave radiation and 250-mb zonal wind; Hartmann and Michelsen 1989, precipitation). The period of oscillation is approximately the same as that of the Madden–Julian oscillation (MJO; Madden and Julian 1971, 1972), also termed the intraseasonal oscillation (ISO).

Climatologically, the ISO is strongest during the boreal winter and spring seasons when it appears as a predominantly eastward propagating large-scale system of convection along the equator, extending from the Indian Ocean east to the dateline (Hendon and Salby 1994). During the south Asian monsoon season, the ISO is typically weaker and of more complex character (Madden 1986). A fundamental and unique characteristic of the summer ISO is a northward movement of convection, beginning in the central equatorial Indian Ocean and ending near the foot of the Himalaya Mountains in northern India. The northward movement of

Corresponding author address: David M. Lawrence, Program in Atmospheric and Oceanic Sciences, Campus Box 311, University of Colorado, Boulder, CO 80309-0311.
E-mail: dml@monsoon.colorado.edu

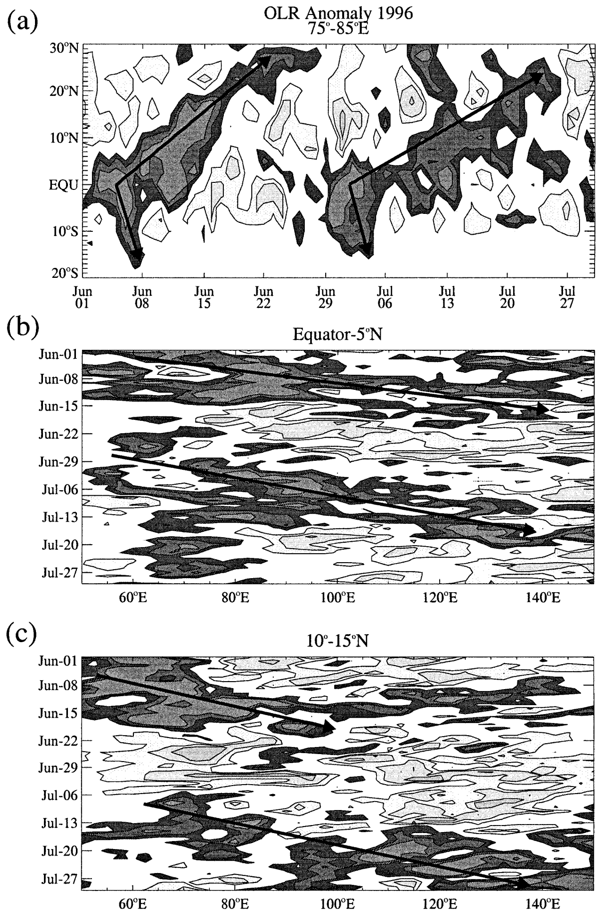

FIG. 1. Time–space diagrams of raw OLR anomalies for Jun–Jul 1996. Anomalies are calculated by removing the mean and the first three harmonics of the annual cycle (365.25, 182.625, and 121.75 days). Contour intervals are every 20 W m^{-2} with dark shades indicating negative OLR anomalies and light shades indicating positive OLR anomalies. OLR anomalies are averaged along (a) 75°–85°E, (b) equator–5°N, and (c) 10°–15°N.

convection has been observed and described by many authors (e.g., Murakami 1976; Yasunari 1979, 1980, 1981; Sikka and Gadgil 1980; Krishnamurti and Subrahmanyam 1982; Singh and Kripalani 1985; Lau and Chan 1986; Wang and Rui 1990). The similarity between the timescale of the ISO and the cycling time from active to break to active period over India led Yasunari (1979), and subsequently Julian and Madden (1981) and Lau and Chan (1986), to suggest that the northward movement of convection is associated with the eastward propagating clouds along the equator (see Madden and Julian 1994 for review). However, Wang and Rui (1990) identify a summertime mode that they describe as an independent northward-moving event that exhibits no eastward movement of convection along the equator and therefore may not be related to the MJO.

These features of the summertime ISO can readily be seen in observations. Figure 1a is a time–latitude section of outgoing longwave radiation (OLR) anomalies along Indian peninsula longitudes, 75°–80°E, during June and July, 1996. Two episodes of coherent northward movement are clearly visible in the raw data. Limited southward movement of convection anomalies is also evident, an additional characteristic of the summertime ISO that has been noted previously by Webster et al. (1998) but has not been investigated. Figure 1b is a time–longitude section along a latitudinal swath between the equator and 5°N. Two eastward propagating convective events occur during the 2-month period. During both events, the northward propagation of convection begins subsequent to the passing of a large-scale equatorial convective system. Eastward movement of convection anomalies in the off-equatorial band 10°–15°N lags the equatorial anomalies by about 5–10 days (Fig. 1c). The off-equatorial eastward movement and the southward movement of convection, which, as will be shown, are robust features of the summertime ISO, have not received much attention in the literature. One of the goals of this study is to interpret this off-equator feature in the context of known ISO dynamics.

A number of theories have been put forth that attempt to explain the northward movement of convection during summer. Webster (1983) and Srinivasan et al. (1993) emphasized the important role of land surface heat fluxes into the boundary layer that destabilize the atmosphere ahead of the ascending zone, causing a northward shift of convective activity. Goswami and Shukla (1984) suggested that the northward propagation is due to a convection–thermal relaxation feedback wherein the convective activity increases static stability while dynamic and radiative relaxation decreases the moist static stability, bringing the atmosphere to a convectively unstable state. Lau and Peng (1990), in a modeling study, found that the interaction between the large-scale monsoon flow and the equatorial intraseasonal oscillation could result in the generation of unstable westward propagating baroclinic disturbances. As these disturbances grow, low-level air would be drawn northward resulting in a rapid northward shift of the area of deep convection. Another interpretation of the northward movement of convection is that, after the equatorial convection arrives in the central equatorial Indian Ocean, the convection splits, with the bulk of the convection redirected northward and southward and the remainder continuing eastward into the western Pacific Ocean (Wang and Rui 1990). Supported by atmospheric model results, Rodwell (1997) hypothesized that breaks in the Indian monsoon can be triggered by injection of dry, high negative potential vorticity air from the Southern Hemisphere midlatitudes. Wang and Xie (1997), based on results of a modeling study of summer ISOs, described the northward "propagation" as a convection "front" formed by the equatorial Rossby waves emanating from the equatorial convection. The Wang and Xie convection front tilts northwestward from the equator to 20°N, resulting in an apparent northward movement as the entire wave packet migrates eastward.

Krishnan et al. (2000) suggest that monsoon breaks are initiated by rapid northwest propagating Rossby waves emanating from convectively-stable anomalies over the Bay of Bengal.

To this point, there is no consensus as to which theory or combination of theories best describes the summertime ISO. While the above theories likely explain important factors that determine the detailed characteristics of the northward movement of convection, they generally fail to address, and cannot be readily extended to explain (except for the theory of Wang and Xie), either the concomitant southward movement of convection into the Southern Hemisphere or the eastward propagation of convection along Indian subcontinent latitudes.

A primary goal of this study is to determine whether eastward propagation of convection along the equator, such as that seen in Fig. 1b, is a prerequisite for northward movement onto the south Asian land mass. If so, can this connection be understood in terms of known ISO dynamics? To this end, it will be useful to compare the evolution of the summer ISO to that of the winter ISO since the winter ISO is typically stronger and exhibits a less complicated evolution.

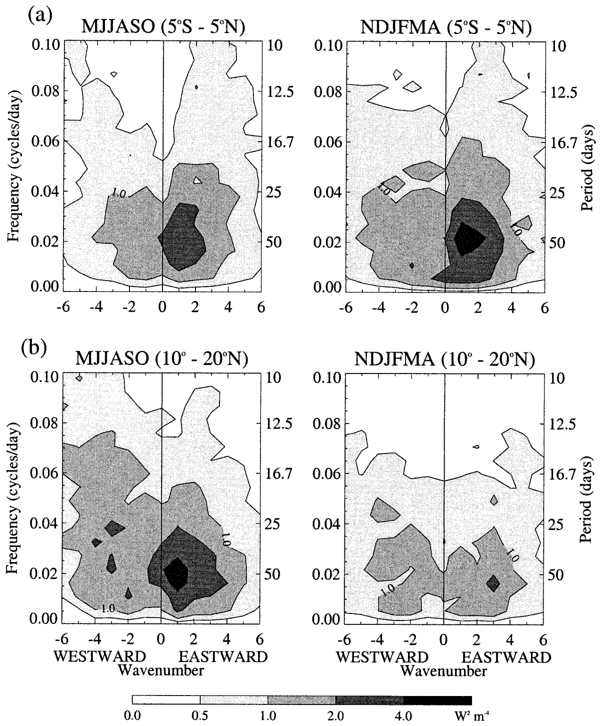

FIG. 2. Average zonal wavenumber-frequency variance spectra of anomalous OLR for 182-day summer (MJJASO) and winter (NDJFMA) seasons. The spectra are averaged over the 24 summers and winters in the record and across the latitude bands (a) 5°S–5°N and (b) 10°–20°N for a total of 120 (24 seasons $\times$ 5 latitude bands) spectra per diagram.

2. Data and methods

a. Data

Two global datasets are used in this study. The National Oceanic and Atmospheric Administration (NOAA) outgoing longwave radiation dataset (Liebmann and Smith 1996) is used to locate areas of deep tropical convection and as a proxy for precipitation (Arkin and Ardanuy 1989). The National Centers for Environmental Prediction (NCEP) and National Center for Atmospheric Research (NCAR) reanalyses (NCEP–NCAR) generated by Kalnay et al. (1996) are employed to represent the circulation at 200, 850, and 1000 mb. Both datasets have 2.5° $\times$ 2.5° spatial resolution while the time resolution is twice daily for OLR and four times daily for the NCEP–NCAR data. Daily averaged values for both OLR and NCEP–NCAR data are used.

ISOs from 24 boreal summers [June to September (JJAS)] during the period 1975–99 are examined. No OLR data were collected during 1978 due to satellite problems, so that year is excluded. In section 3d, ISOs from the 24 boreal winters [December to March (DJFM)] over the same period of record are compared to ISOs from the 24 boreal summers.

b. Wavenumber-frequency spectral analysis

Wavenumber-frequency spectral analysis is used to evaluate the predominant spatial and temporal scales of convection in the south Asian monsoon region. This technique is useful for studying zonally propagating waves (Hayashi 1982) and has previously been employed to investigate convectively coupled equatorial waves by Wheeler and Kiladis (1999), where the technique is described in detail.

The results of a wavenumber-frequency spectral analysis of OLR are shown in Fig. 2. The plots represent an ensemble average of 24 individual wavenumber-frequency spectra generated from 182-day segments representing summer (MJJASO) and for comparison, winter (NDJFMA). Prior to the wavenumber-frequency spectral calculations, the mean, the first three harmonics of the annual cycle, and the linear trend are removed from each 182-day OLR time series and the resulting anomaly time series is tapered to zero at the ends with a 10% cosine taper. Two longitude bands extending around the entire globe are chosen, a swath along the equator (5°S–5°N; Fig. 2a) and a band that crosses the Indian subcontinent and Southeast Asia (10°–20°N; Fig. 2b).

At equatorial latitudes there is a concentration of variance in eastward propagating modes, specifically at eastward wavenumbers 1–3, with periods greater than 25 days. The amplitude is stronger in winter compared to summer as found previously by Madden (1986) and Salby and Hendon (1994). During summer, the low-frequency eastward variance in OLR is also strong across south Asian latitudes (Fig. 2b). The focus of pre-

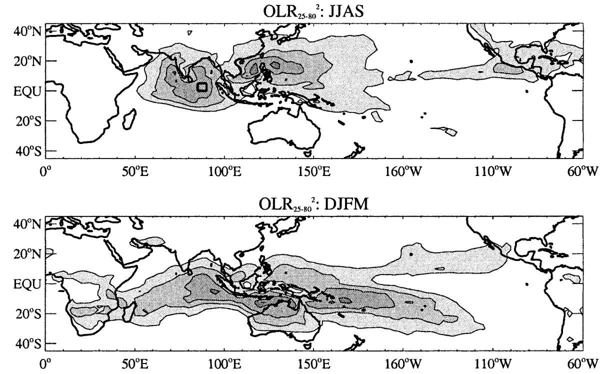

FIG. 3. JJAS and DJFM climatological mean variance maps of 25–80-day bandpass-filtered OLR, contour levels every 100 W^2 m^{-4}.

vious studies has been on the striking northward movement of convection during summer and largely has neglected the eastward movement along Indian subcontinent latitudes.

c. Filtering

To isolate the ISO signal, the OLR and NCEP–NCAR reanalysis fields are filtered with a simple temporal Lanczos bandpass filter with 121 weights (see Duchon 1979), retaining periods between 25 and 80 days. Data filtered in this manner is denoted with a subscript ''25–80'' (e.g., OLR_{25-80}). The results that are shown in this paper are not sensitive to the width of the filter as long as the filter isolates the ISO from the higher-frequency modes that also occur during the boreal summer (e.g., 7–9 days, Lau and Lau 1990; 10–20 days, Krishnamurti and Ardanuy 1980). The mean summer and winter variance maps of the bandpass-filtered OLR_{25-80} are shown in Fig. 3.

d. Lagged cross-correlation and linear regression

A cross-correlation and linear regression technique is used to evaluate the temporal and spatial evolution of circulation and convection patterns associated with the ISO. This technique is the same as that described in detail by Kiladis and Weickmann (1992). Briefly, an area-averaged base region time series is extracted from bandpass-filtered OLR_{25-80}. The base region time series is regressed against identically filtered OLR and 1000-, 850-, and 200-mb u (zonal wind component) and v (meridional wind component) time series at all other grid points. The regression equations are determined based on data from the JJAS monsoon period. The linear dependence of the circulation on deep tropical convection is mapped by applying the regression equation at each grid point relative to a single standard deviation in base region OLR. The temporal evolution of the circulation and convection anomalies is assessed by performing lagged regressions. This method assumes that the relationship between OLR and the circulation is nearly linear, an assumption that is reasonable to the extent that OLR anomalies are linearly related to tropical heating anomalies and that linear dynamics can describe much of the atmospheric response to tropical heating (e.g., Webster 1972; Gill 1980; Sardeshmukh and Hoskins 1988).

The statistical significance of the local linear relationship between OLR in the base region and the dependent variable at each grid point is determined using the correlation coefficient. If the absolute value of the correlation coefficient between OLR in the base region and the dependent variable at a given grid point exceeds the 5% significance level correlation coefficient, then the regressed value for a -1 standard deviation of OLR in the base region is plotted at that grid point. Similarly, if the absolute value of the correlation between the OLR base region and either the u or the v wind component at a single grid point exceeds the correlation coefficient for the band, the total wind anomaly vector is plotted at that grid point.

3. Results

a. Spatial structure and evolution of the summertime intraseasonal oscillation

The time–space evolution of the summertime ISO is evaluated by completing a cross-correlation and linear regression analysis using area-averaged summertime (JJAS) OLR_{25-80} (see boxed region in Fig. 3 that covers the area 0°–5°N, 85°–90°E, central equatorial Indian Ocean) as the predictive time series. The base region selected here coincides with a local maximum in OLR_{25-80} variance. The results are not highly dependent on the location of the base region as long as it is located within the domain of high OLR_{25-80} variance.

The evolution of the summertime ISO, shown here as lagged regression maps every 4 days in Fig. 4, is similar to the results of Lau and Chan (1986) and Wang and Rui (1990) and is qualitatively consistent with the model results of Wang and Xie (1997). Beginning at lag -8 (not shown) to lag -4 days, an area of convection develops in the central equatorial Indian Ocean while convection is suppressed over the Indian subcontinent. As the equatorial convection begins to move off the equator and onto the Indian subcontinent at lag $+4$ days and onwards, initiating an active period of rainfall, the equatorial convection shifts eastward into the western Pacific Ocean. By the time the convection over India has reached its northernmost extent at lag $+12$ days, the equatorial convection is centered just to the north of Papua New Guinea at around 130°–135°E. By lag $+16$ days, the central equatorial Indian Ocean is marked by suppressed convection and one half of the approximately 40-day cycle is complete. This period of oscillation is consistent with previous results that show that

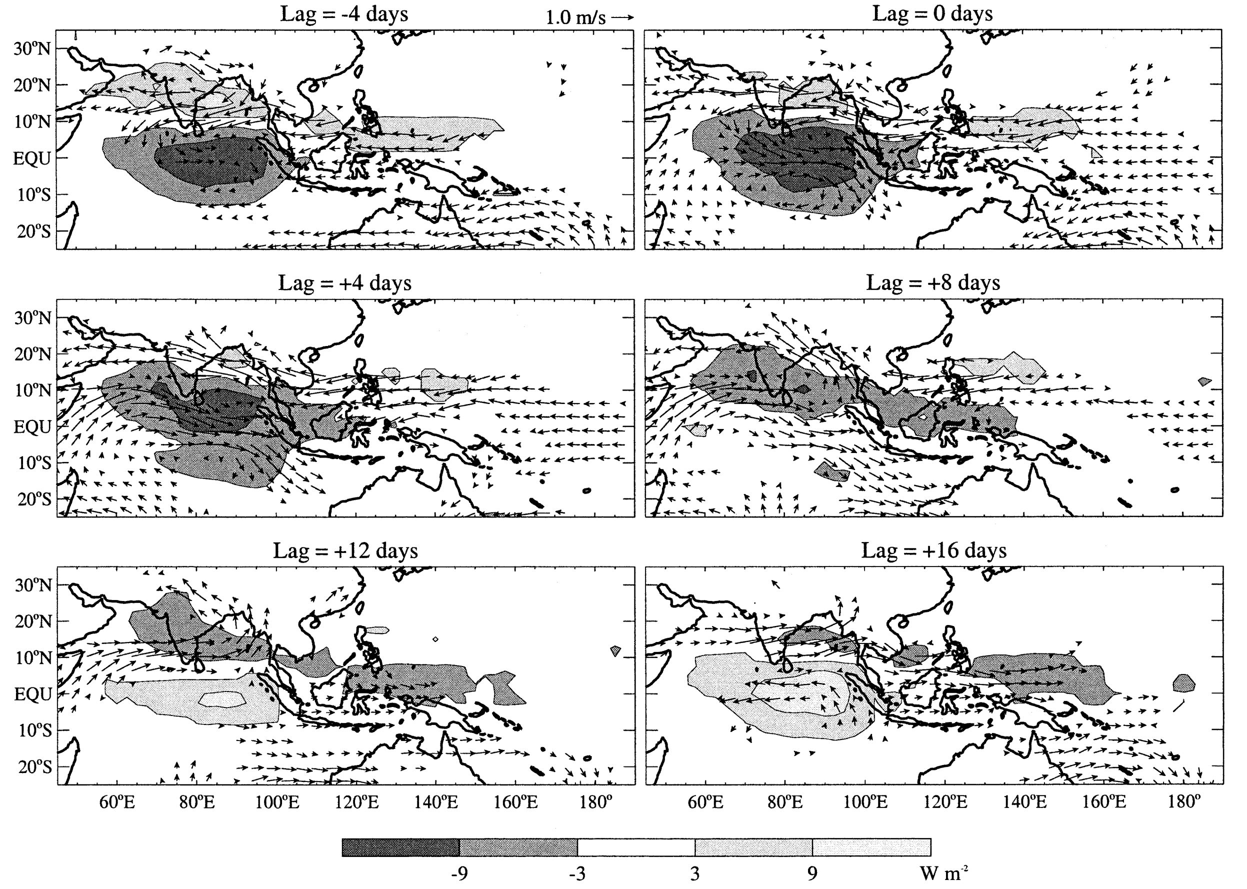

FIG. 4. Lagged regression maps of OLR (shaded) and 850-mb wind (vectors) perturbations relative to a −1 std dev in JJAS OLR_{25-80} in the base region; 0°–5°N, 85°–90°E. All data are bandpass-filtered to retain periods of 25–80 days prior to forming the regressions. Only locally significant OLR anomalies and wind vectors are plotted.

the mean ISO period is shorter during summer relative to winter by about 5–10 days (Hartmann et al. 1992).

At 850 mb, the most prominent feature is the spinup or spindown of the monsoonal circulation relative to the presence of enhanced or suppressed convection over the Indian subcontinent [noted also by Goswami and Mohan (2001)]. During the enhanced ISO convection phase over India (i.e., lag +8 days), the anticyclonic cross-equatorial low-level monsoon gyre is stronger than normal. The off-equatorial convection leads the spinup of the monsoonal circulation by a couple of days (not shown), which suggests that the stronger monsoonal flow may be a response to, rather than an initiator of, the off-equatorial convection.

Time–latitude and time–longitude sections of the regression results along a number of longitudes and latitudes in the Indian Ocean basin are shown in Fig. 5. The dominant feature of the time–latitude sections in Fig. 5a is the northward movement of convection at nearly all longitudes across the Indian Ocean basin. Over India (along 75°E), the northward progression of convection extends to the foothills of the Himalaya Mountains at a rate of about 1.5°–2.0° latitude per day. Along 90°E, the progression of convection is limited to the head of the Bay of Bengal and moves at a somewhat slower rate of around 1.0° latitude per day. The northward movement of convection occurs simultaneously with an eastward movement of convection both along 15°N and, to the east of the maritime continent, along 2.5°N (Fig. 5b). Southward movement of convection from the equator to about 10°–15°S is also observed along 75°E and 90°E. The Southern Hemisphere convection center appears also to propagate eastward, although the sense of the propagation from the time–longitude diagram along 10°S is not conclusive. The southward moving convective anomaly overlies a climatological maxima in summer precipitation south of the equator [not shown, but noted also by Webster et al. (1998)].

Beginning at around lag −8 days the convection appears to develop in situ across much of the Indian Ocean basin rather than propagating from west to east across the basin (Fig. 5b). The in situ development is followed at lag +4 days by eastward propagation into and across the western Pacific Ocean. The apparently in situ development of convection is in contrast to wintertime

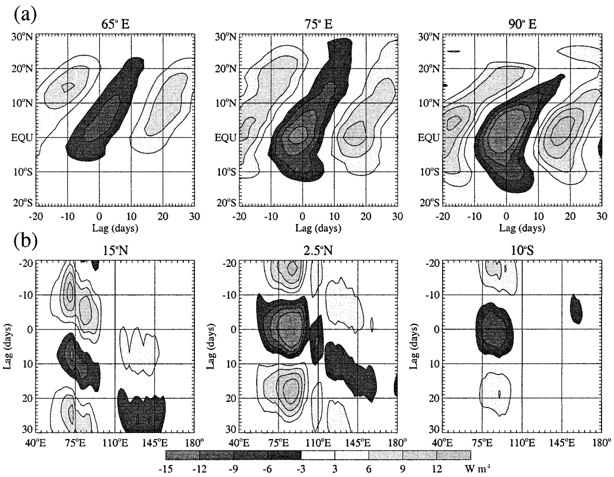

FIG. 5. (a) Lag-latitude diagrams of regressed OLR_{25-80} along 65°E, 75°E, and 90°E. (b) Lag-longitude diagrams of regressed OLR_{25-80} along 15°N, 2.5°N, and 10°S.

ISO behavior when eastward movement of convection clearly dominates at all longitudes (Hendon and Salby 1994).

b. Categorizing intraseasonal oscillations

Since the cross-correlation and linear regression technique employed here is tantamount to compositing about minimums of OLR_{25-80}, it is possible that two or more significantly different types of low-frequency intraseasonal oscillations are integrated together in the regression results. It is possible, therefore, that the apparent link between the northward and eastward movement of convection is simply an artifact of the regression and that the quasi-stationary development of convection reflects the presence of an independent northward moving mode like the one identified by Wang and Rui (1990). Inspection of time–longitude diagrams of individual ISOs (see, for example, Fig. 1) suggests that coherent eastward movement from the Indian Ocean to the western Pacific Ocean does occur in many cases. With an eye towards understanding the initially in situ development of convection followed by the eastward movement of convection, we categorize and composite summertime ISOs according to the relative strength of the eastward versus the westward component of convection along the equator.

The summertime ISOs that will be considered are identified by finding central equatorial Indian Ocean (0°–5°N, 85°–90°E) minimums in $OLR_{25-80ew}$ (OLR filtered to periods between 25 and 80 days and to wavenumbers -6 to $+6$ to emphasize the large-scale low-frequency nature of the ISOs). Fifty-eight events are identified over the 24 summer seasons considered, which translates to an average of just over two ISOs per monsoon season, a frequency that is slightly fewer than previous estimations of the average number of ISOs

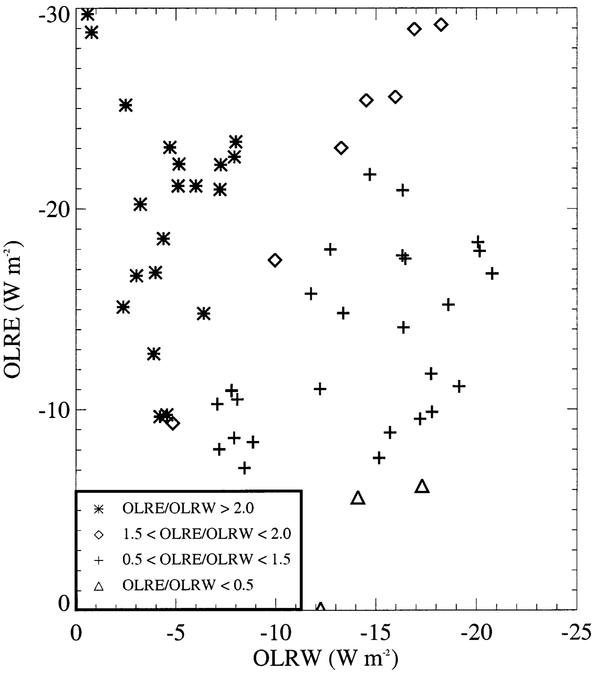

FIG. 6. OLR filtered to periods 25–80 days and wavenumbers 1–6 (large-scale eastward) and -6 to -1 (large-scale westward) and then averaged over the base region (0°–5°N, 85°–90°E) to generate OLRE and OLRW values, respectively. OLRE vs OLRW plotted for each ISO date. ISO date is determined by finding minimums in area-averaged base region OLR that is filtered to periods 25–80 days and wavenumbers -6 to 6. Minimums that are more than 1 std dev below the mean are considered ISO dates.

per summer season (Wang and Rui 1990; Webster et al. 1998).

The ratio of the large-scale eastward component of convection (OLR filtered to periods between 25 and 80 days and wavenumbers 1–6; OLRE) over the large-scale westward component of convection (OLR filtered to periods between 25 and 80 days and wavenumbers -6 to -1; OLRW) is calculated for each of the 58 ISOs. The ISOs subsequently are separated based on the following criteria (see Fig. 6):

- OLRE/OLRW $>$ 2.0 (21 events, denoted ISO_E for eastward movement),
- OLRE/OLRW $>$ 0.5 and OLRE/OLRW $<$ 1.5 (27, denoted ISO_S for in situ development), and
- OLRE/OLRW $<$ 0.5 (3, denoted ISO_W for westward movement).

Of the original 58 ISOs, 7 ISOs with an OLRE/OLRW ratio between 1.5 and 2.0 are removed from the pool to highlight the differences between the two predominant types of ISOs. The three ISOs that exhibit a much stronger westward than eastward convection component are also removed, leaving a total of 48 ISOs that will be considered in composite analyses. The cutoff ratio values were chosen subjectively but were selected with

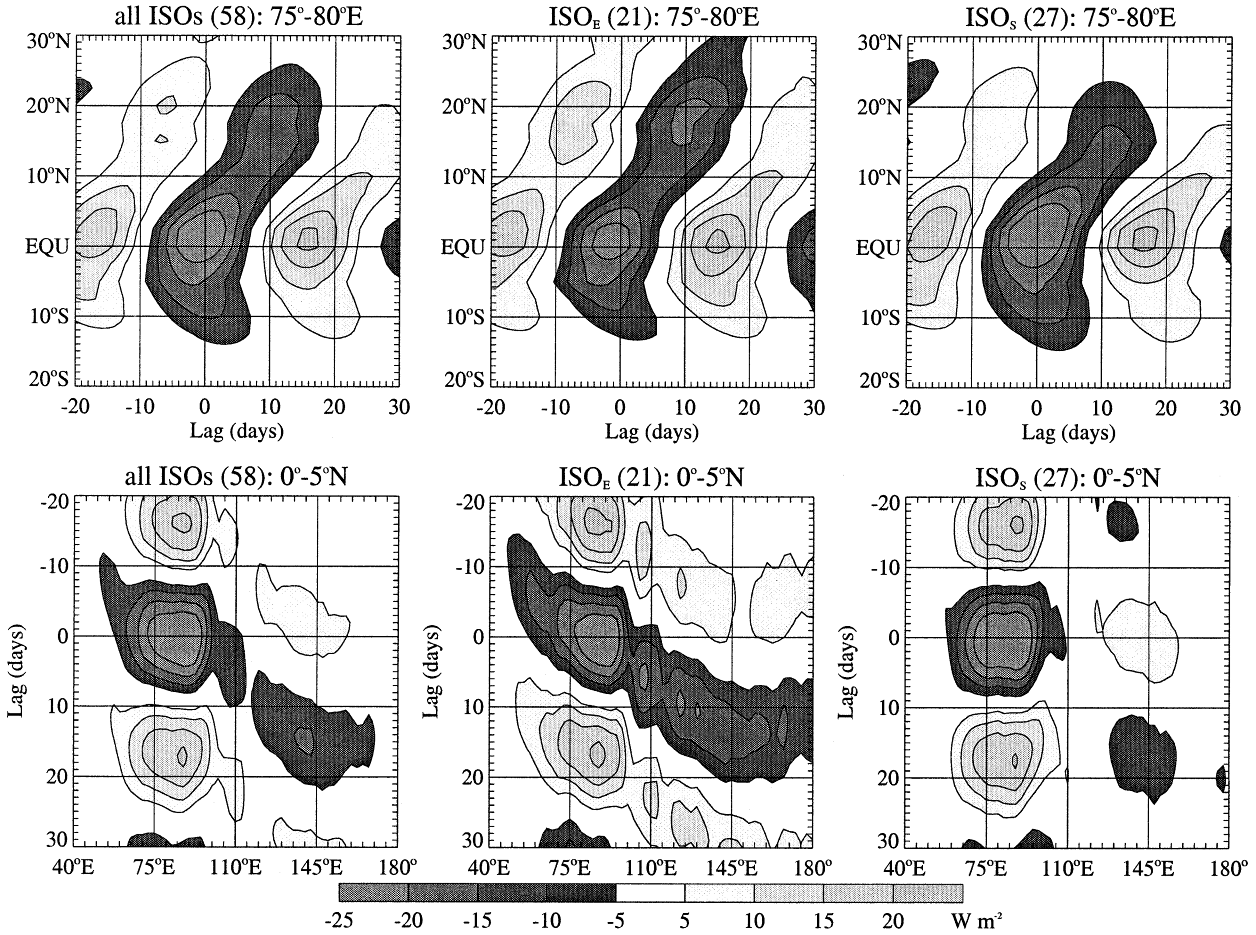

FIG. 7. Lag-latitude sections along 75°–80°E and lag-longitude sections along 0°–5°N of composited OLR25–80. From left to right, composite categories are all ISOs, ISO_E, and ISO_S, as defined in the text.

the goal of separating the clearly coherent eastward-moving cases from those where the eastward movement was less clear or absent. Note also that, despite their relatively balanced eastward and westward components of large-scale convection, which is often an indication of stationary wave activity, the ISO_S events should not necessarily be considered stationary. At this point, it is only known based on the selection criteria that the ISO_S events exhibit in situ development of convection in the central equatorial Indian Ocean. We show subsequently that in nearly all cases, after the initial stationary development, the centers of convection eventually move northward and/or eastward from the region of origin. Furthermore, we are not arguing that the different types of ISOs identified by this separation technique necessarily represent unique modes of variability. The separation of ISOs into the ISO_E and ISO_S categories simply allows us to examine potentially different evolutions of ISOs, which may lead to a better understanding of the summertime low-frequency intraseasonal oscillations.

Lagged composite time–longitude and time–latitude diagrams of $OLR_{25–80}$ are shown in Fig. 7 for all ISOs, ISO_E, and ISO_S events, respectively. The time–longitude and time–latitude sections for the all ISOs category appear very similar to those of Fig. 5 confirming the similarity between the regression and compositing methods. Both types of ISOs, ISO_E and ISO_S, are characterized by northward movement of convection, although ISO_E events tend to propagate about 5°–10° further north on average than the ISO_S events. ISO_E events are also characterized by much stronger and more coherent eastward movement along the equator into the western Pacific Ocean.

By definition, ISO_S events develop in situ in the central equatorial Indian Ocean. They are also characterized by coherent northward movement of convection but only exhibit a weak eastward moving convection anomaly at 10–20 day lags in the western Pacific Ocean. A visual inspection of individual ISO_S events, however, revealed that many ISO_S events, contrary to the composite results, actually do exhibit notable eastward-moving convection anomalies in the western Pacific Ocean. To evaluate the importance of western Pacific Ocean convection anomalies on the northward movement of convection over India, the ISO_E and ISO_S events are further stratified into the following categories:

TABLE 1. Number of ISOs falling into each ISO category as defined in the text. Column heading *N* stands for northward movement of convection onto Indian subcontinent, *E* stands for eastward movement into western Pacific, *NE* stands for both northward movement and eastward movement. $ISO_{E/S}$ represent the ISOs that were initially thrown out to enhance the separation between ISO_E and ISO_S events.

Category	Total	*NE*	*N*	*E*
ISO_E	21	19	2	0
ISO_S	27	17	9	1
ISO_W	3	0	0	0
$ISO_{E/S}$	7	6	1	0

- events followed by northward movement of convection onto the Indian subcontinent and no eastward movement into the western Pacific Ocean (ISO_{EN} or ISO_{SN}),
- events followed by eastward movement of convection into the western Pacific Ocean and no northward movement onto the Indian subcontinent (ISO_{EE} or ISO_{SE}), or
- events followed by both northward movement of convection and eastward movement of convection (ISO_{ENE} or ISO_{SNE}).

The results of the categorization are summarized in Table 1. The vast majority (19 out of 21) of ISO_E events fall into the ISO_{ENE} category. Of the 27 ISO_S events, 17 are ISO_{SNE} events, 9 are ISO_{SN} events, and only 1 is an ISO_{SE} event. Six out of the seven ISOs that were removed from the pool earlier to enhance the clarity of the composites, fall into the northward and eastward category. Thus, the majority (42 out of 54, or 78%) of summertime ISOs that exhibit northward movement also exhibit eastward propagation of convection into the west Pacific Ocean from the equatorial Indian Ocean.

Composite lag-latitude and lag-longitude sections for the ISO_{ENE}, ISO_{SNE}, and ISO_{SN} categories are shown in Fig. 8. By definition, the ISO_{SN} events do not exhibit any convection anomalies in the western Pacific Ocean. Interestingly, the northward movement, while still apparent, is significantly weaker for the ISO_{SN} events than for the other cases. The ISO_{ENE} and ISO_{SNE} events are similar in many ways with both categories exhibiting northward movement across the Indian subcontinent, eastward propagation along the equator in the western Pacific Ocean, and eastward movement along 15°N. The primary difference between the two types is the absence of a significant convection anomaly over the maritime continent for ISO_{SNE} events.

Some characteristics of the three most common ISO types (ISO_{ENE}, ISO_{SNE}, and ISO_{SN}) are listed in Table 2. The speed of northward movement is individually estimated for each individual ISO based on time–latitude diagrams of $OLR_{25–80}$. The average ISO_{ENE} event moves northward about 0.5° day^{-1} faster than the average ISO_{SNE} event (1.9° day^{-1} vs 1.4° day^{-1}). In addition, the convection reaches 145°E about 5 days earlier on average for ISO_{ENE} events compared to ISO_{SNE} events, which indicates that the rate of eastward movement may be related to the rate of northward movement. The eastward and northward phase speeds of individual ISO_{ENE} events correlate at about 0.6, although our confidence in that value is low due to difficulties in accurately determining the northward and eastward phase speeds of individual events.

ISO_{ENE} events are slightly stronger than ISO_{SNE} events with a mean minimum OLR value in the base region of 177 W m^{-2} compared to 183 W m^{-2}. ISO_{ENE} events progress a little further to the north compared to ISO_{SNE} events (31°N versus 25°N). On average, ISO_{ENE} events tend to occur slightly earlier in the monsoon season than ISO_{SNE} events although the histogram of start dates shown in Fig. 9 suggests that the two primary types of ISOs occur with relatively equal regularity across the monsoon season.

To summarize, the composite results, based on the categorization of ISOs according to their propagation characteristics, suggest that the extent, coherence, and speed of the northward movement are directly related to the extent and speed of the eastward movement along the equator. Two questions remain, however. 1) Do the two predominant types of summertime ISOs identified here (ISO_{ENE} and ISO_{SNE}) represent fundamentally different modes of summertime intraseasonal variability or are they simply different manifestations of the same mode? 2) What is the physical mechanism through which the northward and eastward movement of convection are linked? These questions will be addressed in the following two sections.

c. Comparison of ISO_{ENE} and ISO_{SNE} events

As noted above, ISO_{ENE} and ISO_{SNE} events are similar in terms of their convective signature in many ways. They both exhibit northward movement of convection and eastward movement along 15°N as well as eastward propagation of convection from 120° to 170°E. The primary difference between the two types of ISOs is the absence of a convective signal over the maritime continent for ISO_{SNE} events. Similarities between the two categories are also seen in other fields. Time–latitude sections of composited 1000-mb divergence and time–longitude sections of composited 200-mb winds and are shown in Fig. 8 (line contours). Differences between the two primary categories of ISOs in these dynamic fields are small. In both cases, the 1000-mb divergence fields exhibit convergence leading the northward moving convection anomalies by a few days. The upper-level winds are marked, in both cases, by eastward-propagating easterly anomalies ahead of the equatorial convection and westerly anomalies trailing the convection.

Figure 10 shows time–longitude and time–latitude sections of composites of the total unfiltered OLR fields for ISO_{ENE} and ISO_{SNE} events. The two time–latitude

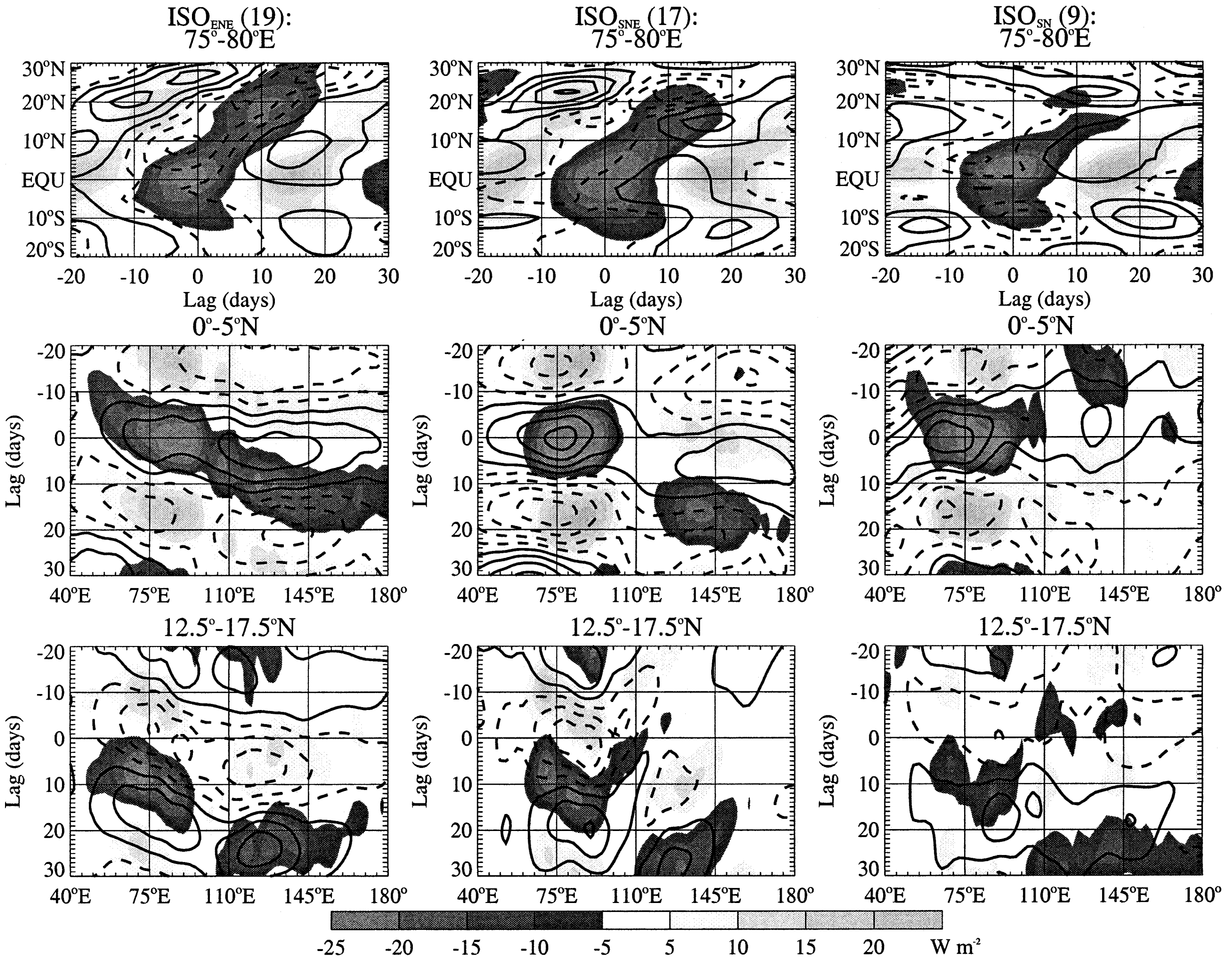

FIG. 8. Same as Fig. 7, except for composites of ISO$_{ENE}$, ISO$_{SNE}$, and ISO$_{SN}$ events as defined in the text. Also shown as lined contours are 1000-mb divergence (top panels), 200-mb zonal wind (middle panels), and 850-mb zonal wind (bottom panels). For 1000-mb divergence, dashed lines indicate convergence, solid lines indicate divergence with a contour interval of 5×10^{-7} s^{-1}. For 200-mb zonal wind and 850-mb zonal wind, solid contours indicated westerly winds and dashed contours indicate easterly winds with contour intervals of 1.0 m s^{-1}. The zero contour is omitted in all fields.

sections are nearly indistinguishable apart from a slightly slower northward movement of convection for ISO$_{SNE}$ events. The time–longitude sections along the equator give a sense of coherent eastward movement for both ISO$_{ENE}$ and ISO$_{SNE}$ events with the main difference between the two being a slower propagation speed for ISO$_{SNE}$ events. Convection between 100° and 120°E is relatively steady across all lags for both ISO$_{ENE}$ and ISO$_{SNE}$ categories.

Lagged time series of composited total OLR and OLR$_{25–80}$ are shown in Fig. 11 at three locations: the central equatorial Indian Ocean (left column), the maritime continent (center), and the western Pacific Ocean (right). In the Indian Ocean and the western Pacific Ocean regions, the total OLR time series undergo significant changes across the ISO cycle, which correspond to large amplitude oscillations in the OLR$_{25–80}$ time series. Over the maritime continent, however, the amplitude of variation in the total OLR fields is small, especially for ISO$_{SNE}$ events, which is reflected in the

TABLE 2. Some characteristics of the three major ISO categories.

	ISO$_{ENE}$	ISO$_{SNE}$	ISO$_{SN}$
No. of events	19	17	9
Min OLR (W m^{-2})	177 ± 28	183 ± 22	1996 ± 35
Northward phase speed along 75°–80°E (°day^{-1})	1.9 ± 0.5	1.4 ± 0.3	1.0 ± 0.3
Max northern extent along 75°–80°E	31° ± 5°N	25° ± 5°N	14° ± 5°N
Avg start date	6 Jul	2 Aug	2 Aug

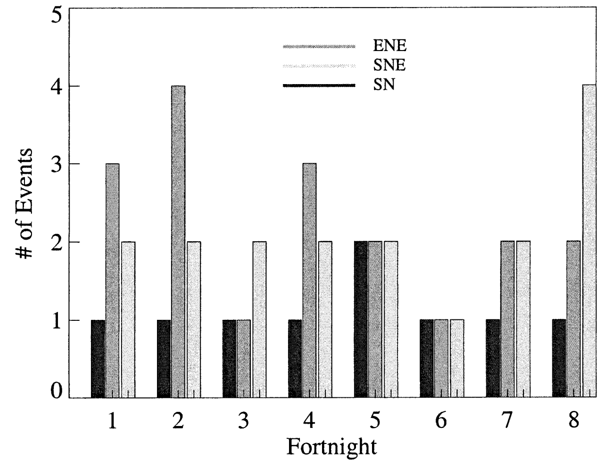

FIG. 9. Histogram of the number of times each of the three most common types of ISOs identified in this study (ISO_{ENE}, ISO_{SNE}, ISO_{SN}, as defined in the text) occur during each of the 10 two-week periods that make up the monsoon season (15 May to 30 Sep).

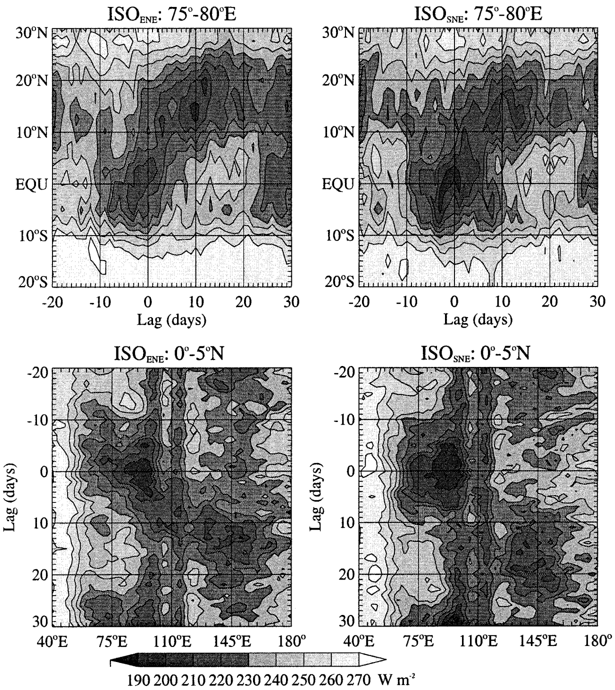

FIG. 10. Same as Fig. 7, except for composites of total OLR fields for ISO_{ENE} (left panels) and ISO_{SNE} (right panels) events.

$OLR_{25–80}$ time series. Since the mean total OLR value for ISO_{SNE} events is about 5–10 W m^{-2} less than for ISO_{ENE} events during the suppressed phase of the oscillation over the maritime continent, the corresponding $OLR_{25–80}$ variations are about 5–10 W m^{-2} smaller, rendering them insignificant; however, the total OLR values during the time period when the ISO is active over the maritime continent (lag +5 days) are approximately the same between event types. This result suggests that the absence of a convection anomaly in the $OLR_{25–80}$ fields over the maritime continent for ISO_{SNE} events is a result of the steady convection that occurs there.

Zhang and Hendon (1997) showed that the absence of a clear signal of anomalous ISO convection over the maritime continent can lead to the incorrect interpretation that the ISO has a strong stationary component. The evidence presented here suggests that ISO_{SNE} events do not exhibit truly stationary behavior and that the ISO_{ENE} and ISO_{SNE} events are likely not distinct modes with different physical mechanisms responsible for their evolution. It is interesting to note, however, that the presence of convection over the maritime continent prior to the initiation of an ISO (i.e., as seen in ISO_{SNE} events) may influence the eastward propagation speed of the ISO, tending to slow the eastward shift of equatorial convection through the Maritime Continent region.

d. Mechanism for northward movement

Since the eastward propagation of convection is a fundamental feature of the majority of summertime ISOs and since the eastward movement is also a characteristic feature of the wintertime ISO, it is reasonable to think of the summertime ISO in the context of known wintertime ISO dynamics. In general, the wintertime ISO is simpler to understand due to its less complicated evolution, which is characterized predominantly by eastward propagation without significant poleward movement, especially across the Indian Ocean basin.

The life cycle of the wintertime ISO has been described by many authors (see, e.g., Knutson and Weickmann 1987; Hendon and Salby 1994). The convection center moves steadily eastward, at approximately the same speed as it does during summer, driven to the east, at least in part, by surface equatorial convergence that leads the convection (Wang and Rui 1990; Maloney and Hartmann 1998). Large-scale cyclonic and anticyclonic gyres dominate the upper level anomalous circulation patterns associated with the wintertime ISO with cyclonic gyres flanking the equator to the west of the suppressed convection and anticyclonic gyres located to the west of enhanced convection with gyres of opposite sense but smaller amplitude apparent at 850 and 1000 mb (Weickmann et al. 1985; Madden 1986; Hendon and Salby 1994). These gyres reflect the Rossby wave response to imposed equatorial heating (Webster 1972; Gill 1980; Sardeshmukh and Hoskins 1988). Since the ISO convection in winter (and hence the latent heating) is centered only slightly south of the equator, the Rossby wave response is nearly symmetric about the equator with Rossby cells of approximately equal amplitude positioned at 25° latitude in either hemisphere.

During summer, the upper level Rossby cells, while still apparent, are not as strong or clearly defined as they are during winter (Knutson and Weickmann 1987). In particular, the Rossby cells in the Northern Hemisphere are difficult to discern in the NCEP–NCAR data. The lack of definition in the Northern Hemisphere may be

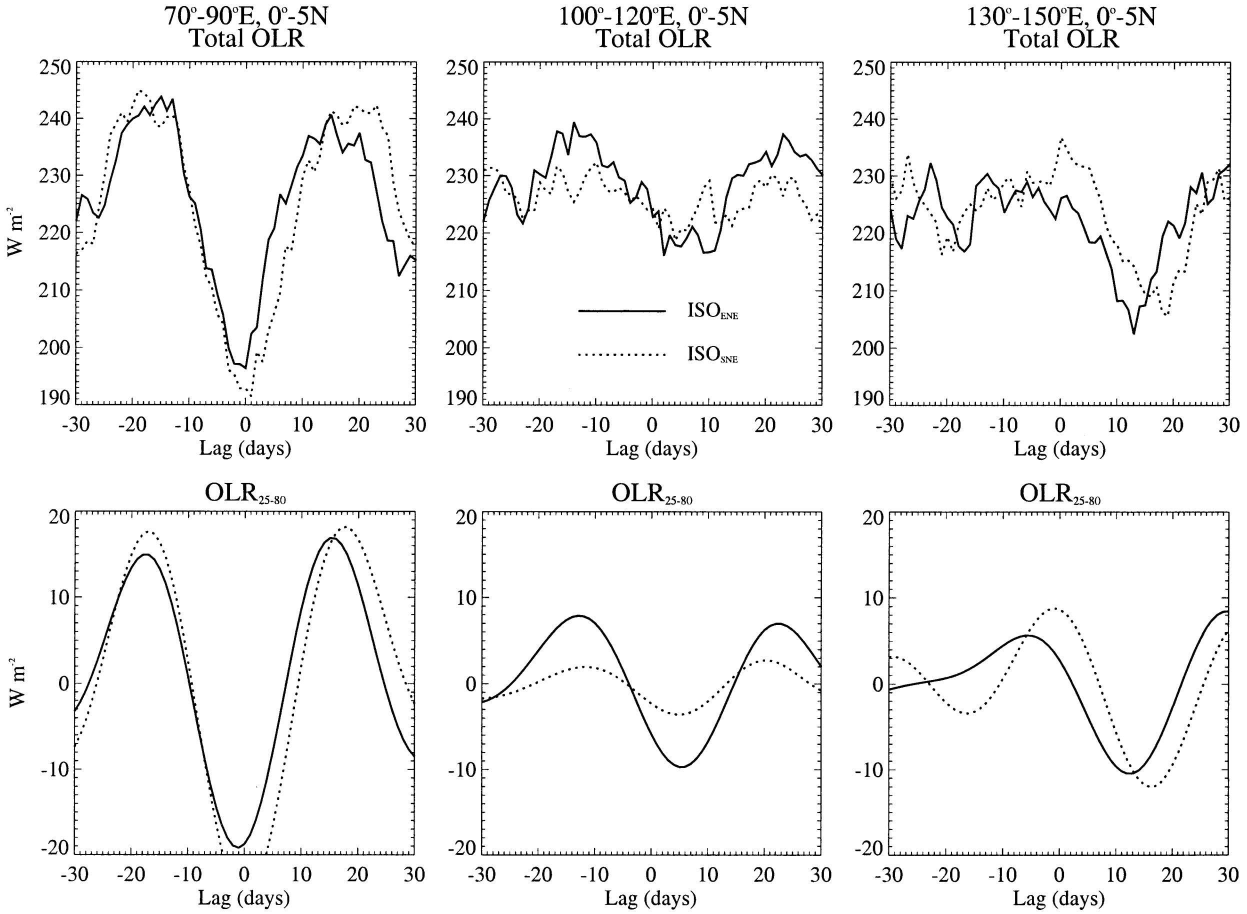

FIG. 11. Lagged time series of composited total OLR (upper panels) and OLR_{25-80} (lower panels) for ISO_{ENE} (solid lines) and ISO_{SNE} (dashed lines) events. Time series are shown for central Indian Ocean, the maritime continent, and the western Pacific Ocean.

due to the complicated summertime ISO convection pattern, which includes both the equatorial convection and the northwestward-oriented off-equatorial band of convection. Consequently, a direct comparison of the summertime ISO circulation to that of the Gill (1980) model is not practical since the circulation response to the equatorial heat source is superimposed by the circulation response to the off-equatorial heat source. Nonetheless, the Rossby cells observed south of the equator support the theory that the summertime equatorial ISO convection excites trailing Rossby cells in both hemispheres.

For both summer and winter ISOs, time–latitude sections along 90°E of the regressed 1000-mb divergence fields (divergence filtered to retain periods 25 to 80 days prior to forming the regression) are shown contoured over the regressed OLR_{25-80} values in Fig. 12. Equatorial convergence that leads the convection is apparent in both seasons and has been ascribed previously to frictionally dominated boundary layer convergence onto the equator that is associated with the Kelvin component easterlies (Wang and Rui 1990; Maloney and Hartmann 1998). In addition, a meridional component of convergence is seen at the base of the Rossby cells in both hemispheres and during both seasons that peaks at about 15°. The strength of the convergence is asymmetric towards the summer hemisphere, which is caused partly by cross-equatorial surface flow into the summer hemisphere, predicted by the Gill (1980) response to off-equatorial heating, to the west of the heat source (Madden 1986). In addition, when the heating is focussed in one hemisphere (as it is during summer), the Rossby cell of the same hemisphere is amplified, which leads to stronger surface convergence within that Rossby cell.

For summertime ISOs, the northern off-equatorial convergence anomaly leads the convection anomaly by a few days, implying that the convection advances northward into the region of off-equatorial surface convergence in much the same way that the equatorial convection maintains its eastward propagation by shifting into the equatorial surface convergence. In winter, however, despite the remarkably similar meridional pattern of convergence (inverted about the equator), no analogous poleward movement of convection is observed. The dissimilar, and not simply opposite, climatological-base states between seasons may explain why poleward movement of convection is observed during summer but

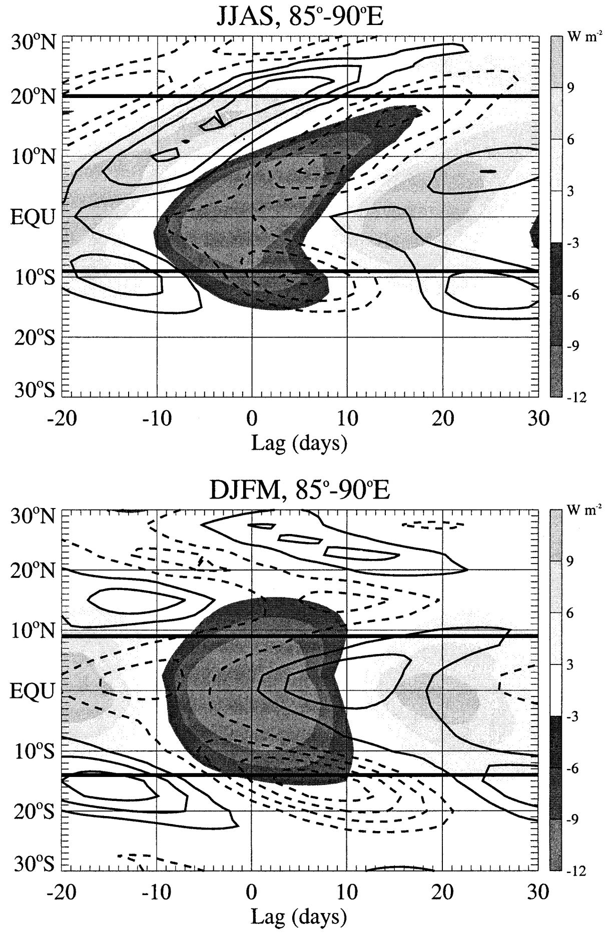

FIG. 12. Lag-latitude diagrams along 85°–90°E of regressed OLR (shaded) and 1000-mb divergence (contours). Divergence contour interval is 3×10^{-7} s^{-1} with the zero contour omitted. Dashed lines indicate negative divergence or convergence. Thick black lines indicate latitude of seasonal mean 28°C isotherm both north and south of the equator at 85°–90°E.

not during winter. During winter, mean SSTs greater than 28°C extend south to only about 10°–15°S across the Indian Ocean basin, whereas during summer, warm SSTs envelop the entire northern Indian Ocean waters including the entire Bay of Bengal and a sizeable portion of the Arabian Sea. Therefore, since deep convection tends to develop over regions of warm SST (a necessary but not sufficient condition for deep convection) and is suppressed over areas of cool SST, no southward movement of convection is observed during northern winter despite the strong surface convergence. Along 85°–90°E, for example, SSTs in excess of 28°C are confined to areas north of around 13°S in the wintertime but extend clear across the Bay of Bengal to near 20°N during summertime (see Fig. 12).

Seasonal differences in low-level monsoonal flow may also be a factor conspiring against southward movement of ISO convection in winter. During summer, the southwesterly flow into the Asian monsoon region transports moisture from the Southern Hemisphere and the Arabian Sea, fuelling the monsoon rainfall (Cadet and Greco 1987). The winter monsoon flow is not as well developed, does not extend as far south as its summer counterpart, and is not as moisture laden leaving the area of off-equatorial convergence located at 15°S without a steady external source of water vapor.

4. Summary and discussion

By separating summertime ISOs based on their zonal propagation characteristics in the Indian Ocean and the western Pacific Ocean, we have shown that the eastward propagation of convection along the equator is a fundamental feature of the majority of summertime ISOs (42 out of the 54 ISOs that exhibit northward movement, or 78%). The eastward propagation appears to be directly related to the northward movement of convection that is associated with active and break cycles of precipitation across India. Previous diagnostic studies, using significantly less data, have also determined that there may be a link between the eastward and northward movement (e.g., Yasunari 1979; Julian and Madden 1981; Knutson and Weickmann 1987).

Wang and Rui (1990) identified a summertime mode that appears to be an independent northward-moving event that does not exhibit any associated eastward movement. Our results suggest that this type of ISO occurs rarely (only 12 out of 54 summertime ISO events considered here exhibit northward movement without eastward movement along the equator) and is characterized by relatively stunted northward movement. According to Wang and Rui, this type of mode occurred 13 times in the Indian Ocean sector over the period 1975–85 (which corresponds to a nearly threefold larger frequency compared to our results). It is possible that the discrepancy between our results and those of Wang and Rui is caused in part by the frequent absence of a strong convection anomaly over the maritime continent, which can be masked by the steady convection there (see Fig. 11). This gap in the convection anomaly signal could lead to the interpretation that the northward movement is independent from eastward movement when the two may not actually be independent.

Eastward movement of convection along Indian subcontinent latitudes is also found to be a recurring feature of summertime ISOs. This eastward movement, combined with the equatorial eastward propagation and the northward movement leads to the complete interpretation that summertime ISO convection appears as a band, tilting northwestward with latitude and stretching from the equator to about 20°N, that moves coherently to the east (see Figs. 4 and 5). Viewed along any meridian, the convection anomaly appears to propagate northward (e.g., in a time–latitude section) while the entire system moves to the east. This conceptual viewpoint is supported by the result that the extent and rate of northward propagation is linearly related to the extent and rate of eastward propagation along the equator.

Evidence of similar wavelike processes for both summer and winter ISOs suggests that their existence and basic evolution are the result of similar dynamical processes and that the predominant type of summer ISO is not a unique mode of variability. Instead, the summertime ISO can be thought of as a wintertime ISO modified by the basic state. The differences, particularly in terms of the poleward propagation during summer, appear to be due primarily to the different underlying basic states. In particular, warm SSTs and the associated moist boundary layer extend far to the north during boreal summer causing the whole of the northern Indian Ocean region to be conditionally unstable. Large-scale surface convergence into the Rossby cell in this conditionally unstable region initiates off-equatorial convection thereby generating the northwestward-oriented band of convection.

Northward movement of convection has also been observed over the western Pacific Ocean (Chen and Murakami 1988; Wang and Rui 1990). While this feature of the summertime ISO has not been examined specifically in this study, the mechanism for northward movement described here may also be appropriate for the western Pacific Ocean northward moving arm of convection, assuming that the equatorial convection proceeds far enough across the Pacific Ocean for the trailing Rossby cells to be located over the western Pacific Ocean. When the equatorial convection dies as it moves over the cooler SSTs of the eastern Pacific Ocean, the Kelvin–Rossby wave packet that is excited by the convection becomes decoupled (Wang and Xie 1997) and the Rossby cells can then propagate to the north and west. These decoupled Rossby waves may be related to the northwestward-moving mode described by Hartmann et al. (1992). Decoupled Rossby waves may also be relevant to the ISO_{SN} mode, which exhibits some northward movement but no eastward movement of convection along the equator, suggesting the Kelvin–Rossby wave packet may be decoupled. A weak hint of westward propagation across India along 15°N is seen in the composite time–longitude diagram for ISO_{SN} events (Fig. 8) but it is difficult to draw definitive conclusions from such a small sample size (nine members).

During winter, distinct poleward propagation of intraseasonal convection is essentially absent except for the occasional southeastward extension of convection into the South Pacific convergence zone (SPCZ; e.g., Wang and Rui 1990). Matthews et al. (1996) showed that intraseasonal convection in the SPCZ is triggered by equatorward advection of large-magnitude potential vorticity (PV) air by the upper-tropospheric anticyclone that is centered over the equatorial convection. The high PV air induces deep ascent to the south and east of the equatorial convection at latitudes between 15° and 30°S. The poleward convection occurs to the east of the equatorial convection, therefore, this mechanism is not analogous to the Rossby cell-induced surface frictional convergence mechanism described in this study, which can only generate poleward propagation to the west of the equatorial convection.

Finally, since most atmospheric general circulation models cannot sustain a realistic eastward moving ISO in summer or winter (Slingo et al. 1996), they cannot, therefore, be expected to accurately simulate the northward movement of convection associated with the active and break cycles of the monsoon. The results of this study emphasize the importance of correctly simulating the eastward moving ISO if progress is to be made in the simulation and prediction of the Asian monsoon.

Acknowledgments. We thank George Kiladis, Bob Grossman, and Bob Tomas for useful comments on an earlier draft of this manuscript. This research was supported by NSF Grant ATM-9526030. OLR, NCEP–NCAR reanalysis, and Reynolds SST data were provided by the NOAA CIRES Climate Diagnostic Center, Boulder, Colorado, from their Web site at http://www.cdc.noaa.gov/.

REFERENCES

Arkin, P. A., and P. E. Ardanuy, 1989: Estimating climatic-scale precipitation from space: A review. *J. Climate,* **2,** 1229–1238.

Cadet, D. L., 1986: Fluctuations of precipitable water over the Indian Ocean. *Tellus,* **38A,** 170–177.

——, and S. Greco, 1987: Water vapor transport over the Indian Ocean during the 1979 summer monsoon. Part I: Water vapor fluxes. *Mon. Wea. Rev.,* **115,** 653–663.

Chen, T.-C., and M. Murakami, 1988: The 30–50 day variation of convective activity over the western Pacific Ocean with emphasis on the northwestern region. *Mon. Wea. Rev.,* **116,** 892–906.

Duchon, C. E., 1979: Lanczos filtering in one and two dimensions. *J. Appl. Meteor.,* **18,** 1016–1022.

Gill, A. E., 1980: Some simple solutions for heat-induced tropical circulation. *Quart. J. Roy. Meteor. Soc.,* **106,** 447–462.

Goswami, B. N., and J. Shukla, 1984: Quasi-periodic oscillations in a symmetric general circulation model. *J. Atmos. Sci.,* **41,** 20–37.

——, and R. S. Ajaya Mohan, 2001: Intraseasonal oscillations and interannual variability of the Indian summer monsoon. *J. Climate,* **14,** 1180–1198.

Hartmann, D. L., and M. L. Michelsen, 1989: Intraseasonal periodicities in Indian rainfall. *J. Atmos. Sci.,* **46,** 2838–2862.

——, ——, and S. A. Klein, 1992: Seasonal variations of tropical intraseasonal oscillations: A 20–25-day oscillation in the western Pacific. *J. Atmos. Sci.,* **49,** 1277–1289.

Hayashi, Y., 1982: Space–time spectral analysis and its application to atmospheric waves. *J. Meteor. Soc. Japan,* **60,** 156–171.

Hendon, H. H., and M. L. Salby, 1994: The life cycle of the Madden–Julian oscillation. *J. Atmos. Sci.,* **51,** 2225–2237.

Julian, P. R., and R. A. Madden, 1981: Comments on a paper by T. Yasunari: A quasistationary appearance of 30- to 40-day period in the cloudiness fluctuations during the summer monsoon over India. *J. Meteor. Soc. Japan,* **59,** 435–437.

Kalnay, E., and Coauthors, 1996: The NCEP/NCAR 40-Year Reanalysis Project. *Bull. Amer. Meteor. Soc.,* **77,** 437–471.

Kiladis, G. N., and K. M. Weickmann, 1992: Circulation anomalies associated with tropical convection during northern winter. *Mon. Wea. Rev.,* **120,** 1900–1923.

Knutson, T. R., and K. M. Weickmann, 1987: 30–60-day atmospheric oscillations: Composite life cycles of convection and circulation anomalies. *Mon. Wea. Rev.,* **115,** 1407–1436.

——, ——, and J. E. Kutzbach, 1986: Global-scale intraseasonal oscillations of outgoing longwave radiation and 250-mb zonal wind during Northern Hemisphere summer. *Mon. Wea. Rev.,* **114,** 605–623.

Krishnamurti, T. N., and P. Ardanuy, 1980: The 10- to 20-day westward propagating mode and ''breaks in the monsoons.'' *Tellus,* **32,** 15–26.

——, and D. Subrahmanyam, 1982: The 30–50-day mode at 850 mb during MONEX. *J. Atmos. Sci.,* **39,** 2088–2095.

Krishnan, R., C. Zhang, and M. Sugi, 2000: Dynamics of breaks in the Indian summer monsoon. *J. Atmos. Sci.,* **57,** 1354–1372.

Lal, M., K. K. Singh, G. Srinivasan, L. S. Rathore, D. Naidu, and C. N. Tripathi, 1999: Growth and yield responses of soybean in Madhya Pradesh, India to climate variability and change. *Agric. For. Meteor.,* **93,** 53–70.

Lau, K.-H., and N.-C. Lau, 1990: Observed structure and propagation characteristics of tropical summertime synoptic scale disturbances. *Mon. Wea. Rev.,* **118,** 1888–1913.

Lau, K.-M., and P. H. Chan, 1986: Aspects of the 40–50 day oscillation during the northern summer as inferred from outgoing longwave radiation. *Mon. Wea. Rev.,* **114,** 1354–1367.

——, and L. Peng, 1990: Origin of low frequency (intraseasonal) oscillations in the tropical atmosphere. Part III: Monsoon dynamics. *J. Atmos. Sci.,* **47,** 1443–1462.

Liebmann, B., and C. A. Smith, 1996: Description of a complete (interpolated) outgoing longwave radiation dataset. *Bull. Amer. Meteor. Soc.,* **77,** 1275–1277.

Madden, R. A., 1986: Seasonal variations of the 40–50 day oscillation in the Tropics. *J. Atmos. Sci.,* **43,** 3138–3158.

——, and P. R. Julian, 1971: Detection of a 40–50 day oscillation in the zonal wind in the tropical Pacific. *J. Atmos. Sci.,* **28,** 702–708.

——, and ——, 1972: Description of global-scale circulation cells in the Tropics with a 40–50 day period. *J. Atmos. Sci.,* **29,** 3138–3158.

——, and ——, 1994: Observations of the 40–50 day tropical oscillation—A review. *Mon. Wea. Rev.,* **122,** 814–837.

Maloney, E. D., and D. L. Hartmann, 1998: Frictional moisture convergence in a composite life cycle of the Madden–Julian oscillation. *J. Climate,* **11,** 2387–2403.

Matthews, A. J., B. J. Hoskins, J. M. Slingo, and M. Blackburn, 1996: Development of convection along the SPCZ within a Madden–Julian oscillation. *Quart. J. Roy. Meteor. Soc.,* **122,** 669–688.

Murakami, T., 1976: Cloudiness fluctuations during the summer monsoon. *J. Meteor. Soc. Japan,* **54,** 175–181.

Raghavan, K., D. R. Sikka, and S. V. Gujar, 1975: The influence of cross-equatorial flow over Kenya on the rainfall of western India. *Quart. J. Roy. Meteor. Soc.,* **101,** 1003–1004.

Rodwell, M. J., 1997: Breaks in the Asian monsoon: The influence of Southern Hemisphere weather systems. *J. Atmos. Sci.,* **54,** 2597–2611.

Salby, M. L., and H. H. Hendon, 1994: Intraseasonal behavior of clouds, temperature, and motion in the Tropics. *J. Atmos. Sci.,* **51,** 2207–2224.

Sardeshmukh, P. D., and B. J. Hoskins, 1988: The generation of global rotational flow by steady idealized tropical divergence. *J. Atmos. Sci.,* **45,** 261–278.

Sikka, D. R., and S. Gadgil, 1980: On the maximum cloud zone and the ITCZ over Indian longitudes during the southwest monsoon. *Mon. Wea. Rev.,* **108,** 1840–1853.

Singh, S. V., and R. H. Kripalani, 1985: The south to north progression of rainfall anomalies across India during the summer monsoon season. *Pure Appl. Geophys.,* **123,** 624–637.

Slingo, J. M., and Coauthors, 1996: Intraseasonal oscillations in 15 atmospheric general circulation models: Results from an AMIP diagnostic subproject. *Climate Dyn.,* **12,** 325–357.

Srinivasan, J., S. Gadgil, and P. J. Webster, 1993: Meridional propagation of large-scale monsoon convective zones. *Meteor. Atmos. Phys.,* **52,** 15–35.

Wang, B., and H. Rui, 1990: Synoptic climatology of transient tropical intraseasonal convection anomalies: 1975–1985. *Meteor. Atmos. Phys.,* **44,** 43–61.

——, and X. Xie, 1997: A model for the boreal summer intraseasonal oscillation. *J. Atmos. Sci.,* **54,** 72–86.

Webster, P. J., 1972: Response of the tropical atmosphere to local steady forcing. *Mon. Wea. Rev.,* **100,** 518–541.

——, 1983: Mechanisms of low-frequency variability: Surface hydrological effects. *J. Atmos. Sci.,* **40,** 2110–2124.

——, V. O. Magaña, T. N. Palmer, J. Shukla, R. A. Tomas, M. Yanai, and T. Yasunari, 1998: Monsoons: Processes, predictability, and the prospects for prediction. *J. Geophys. Res.,* **103,** 14 451–14 510.

Weickmann, K. M., G. R. Lussky, and J. E. Kutzbach, 1985: Intraseasonal (30–60 day) fluctuations of outgoing longwave radiation and the 250 mb streamfunction during northern winter. *Mon. Wea. Rev.,* **113,** 941–961.

Wheeler, M., and G. N. Kiladis, 1999: Convectively coupled equatorial waves: Analysis of clouds and temperature in the wavenumber-frequency domain. *J. Atmos. Sci.,* **56,** 374–399.

Yasunari, T., 1979: Cloudiness fluctuations associated with the Northern Hemisphere summer monsoon. *J. Meteor. Soc. Japan,* **57,** 227–242.

——, 1980: A quasi-stationary appearance of 30- to 40-day period in the cloudiness fluctuations during the summer monsoon over India. *J. Meteor. Soc. Japan,* **58,** 225–229.

——, 1981: Structure of the Indian monsoon system with around 40-day period. *J. Meteor. Soc. Japan,* **59,** 225–229.

Zhang, C., and H. H. Hendon, 1997: Propagating and standing components of the intraseasonal oscillation in tropical convection. *J. Atmos. Sci.,* **54,** 741–752.